Elaborately Aligning Bead-Shaped Nanowire Arrays Generated by a Superhydrophobic Micropillar Guiding Strategy

Yuchen Wu, Xiao Chen, Bin Su, Yanlin Song, and Lei Jiang*

Bead-shaped 1D structures are of great interest due to their unique applications in mesoscopic optics/electronics and their specific ability to collect tiny droplets. Here, a novel method to fabricate aligning bead-shaped nanowire arrays assisted by highly adhesive superhydrophobic surfaces based on a micropillar guiding strategy is presented. Different from previous fabrication techniques, bead-shaped nanowires generated in this method are strictly oriented in a large scale. Rayleigh instability, which occurs at ultralow polymer concentration, can introduce bead-shaped nanowires at the cost of structural strength. Thus, PS spheres are more suitable to serve as bead building blocks to generate firm bead-shaped nanowire arrays. The bead number is tunable by tailoring the polystyrene-sphere/polyvinyl-formal ratio. Furthermore, as-prepared bead-shaped nanowires have the unique ability to directionally drive tiny drops and collect coalesced microdroplets when placed in mist. With an increase in humidity, the nanowires show a segmented swelling behavior in the "bead" parts whereas the "joint nanowire" parts remain the same. Because such bead-shaped nanowires are formed regularly, collected microdroplets upon the beads would not interact with each other. The findings offer new insight into the alignment of bead-shaped nanostructures and might provide promising opportunities in fundamental research and for industrial applications.

1. Introduction

Bead-shaped 1D nanostructures, composed of alternate beads and joints, have become the focus of intensive research owing to their unique applications in mesoscopic optics/electronics and specific ability to collect tiny droplets.[1–4] There has been an emerging interest to rationally prepare bead-shaped 1D nanostructures, including self-assembly,[5–8] microfluidic system,[9] solution blowing[10] and electrospinning methods.[11–14] Recently, inspired by the capture silk of cribellate spider, a Rayleigh instability driven wet-rebuilt strategy was proposed by our group to fabricate periodic bead-shaped fibers.[15,16] Notably, such 1D nanostructures generated by existing approaches[5–16] commonly exhibit a disordered alignment with random positions and orientations. For practical applications, highly ordered arrays of these nanostructures might exhibit prior properties that are not found in their disordered counterparts.[17,18] Therefore, it should be of great interest and technological importance to explore a feasible way to align bead-shaped 1D nanostructures in regular patterns.

Highly adhesive superhydrophobic pillar-structured substrates have been reported to successfully guide each nanowire into a designed position in our latest studies.[19,20] Either high-molecular-weight polymer[19] or hydrogen-bonds-driven small molecules[20] has the possibility to form aligning nanowire arrays after the water evaporation from regular liquid bridges. The geometrical location of micropillars decides the alignment of liquid bridges, yielding programmed nanowire patterns. Recently, we found that ultra-low polymer concentration could lead to wet-rebuilt phenomenon occurring during the formation process of ultra-thin nanowires, indicating a possible strategy to generate and position bead-shaped nanowires.

Herein, we report a facile yet effective approach to prepare aligning bead-shaped nanowire arrays upon superhydrophobic pillar-structured surfaces with high adhesion. Ultralow polymer concentration leads to Rayleigh instability during the narrowing of liquid bridges, yielding oriented bead-shaped nanowire arrays at the cost of structural strength. In order to generate firm bead-shaped nanowires, polystyrene (PS) spheres have been introduced to serve as bead building blocks. Furthermore, bead-shaped nanowires own the unique ability to directionally drive tiny drops and collect coalesced microdroplets when placed in mist. Following the increase of environmental humidity, the nanostructures show a segmented swelling behavior in the "bead" parts whereas the "joint nanowire" parts remain the same. Our findings offer new insights into the alignment of bead-shaped nanowires and might provide promising opportunities in fundamental research and for industrial applications.

Dr. Y. C. Wu, Dr. B. Su, Prof. Y. L. Song, Prof. L. Jiang
Beijing National Laboratory for Molecular Sciences (BNLMS)
Key Laboratory of Organic Solids
Institute of Chemistry
Chinese Academy of Sciences (ICCAS)
Beijing, 100190, P. R. China
E-mail: subin0000@iccas.ac.cn
Dr. X. Chen, Prof. L. Jiang
School of Chemistry and Environment
Beihang University
Beijing, 100191, P. R. China

DOI: 10.1002/adfm.201200971

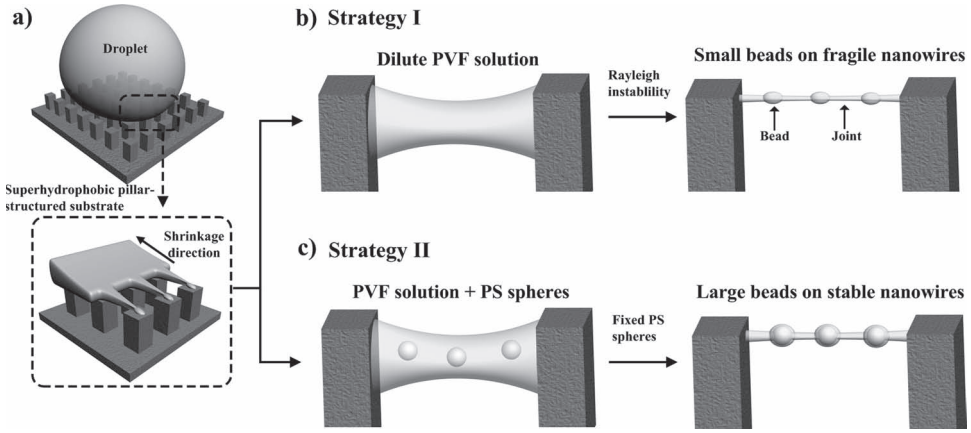

Figure 1. Schematic illustration of generating aligned bead-shaped nanowire arrays on a highly adhesive superhydrophobic pillar-structured substrate. The bead-shaped structure can be introduced by either Rayleigh instability or rigid PS spheres. a) A PVF droplet pinned firmly upon the anti-wetting surface, exhibiting a transitional superhydrophobic state between Wenzel's and Cassie's states. Following the evaporation of water, regular liquid bridges connecting neighbor micropillars were generated after the unidirectional shrinkage of three phase contact line. b) Pure ultralow polymer concentration leads to Rayleigh instability occurring upon the liquid bridges, yielding bead-shaped nanowires at the cost of structural strength. c) Rigid PS spheres can be introduced into the liquid bridges, serving as bead building blocks to prepare firm bead-shaped nanowire arrays.

2. Results and Discussion

Figure 1 demonstrates the detailed formation process of aligning bead-shaped nanowire arrays. A high-adhesively superhydrophobic pillar-structured substrate with water contact angle as high as 151.4° ± 1.1° and a 39° sliding angle was prepared through a steam-modification method.[19] A polyvinyl-formal (PVF) droplet pinned firmly upon this microstructured surface, exhibiting a transitional superhydrophobic state between Wenzel's and Cassie's states.[21] Regular liquid bridges connecting neighbor micropillars were generated following the unidirectional shrinkage of three phase contact line (TCL). Then, two strategies have been proposed to form bead-shaped nanowire arrays. One is to decrease the polymer concentration until Rayleigh instability occurs upon the wet nanowires (Figure 1b), and the other way is directly employing rigid PS spheres as building blocks for the bead generation (Figure 1c).

2.1. Fragile Bead-Shaped Nanowire Arrays Induced by Rayleigh Instability

With the evaporation of water, long-chain PVF molecules inside liquid bridges began to wrap with each other, yielding strong structural cohesive force to fight against destructive capillary force.[19] When the polymer concentration was ultra-low, local molecular aggregations might occur due to the Rayleigh instability.[22] Thus, bead-shaped nanowires could be formed. **Figure 2**b shows the top view scanning electron microscope (SEM) image of aligning bead-shaped nanowire arrays generated at 10^{-8} (w/w) solution concentration. Horizontally oriented 1D nanostructures could be found over the whole image, indicating well guiding effect of adhesively superhydrophobic pillar-structured surfaces. From magnified image shown in Figure 2c, one bead-shaped nanowire was bridging neighbor micropillar

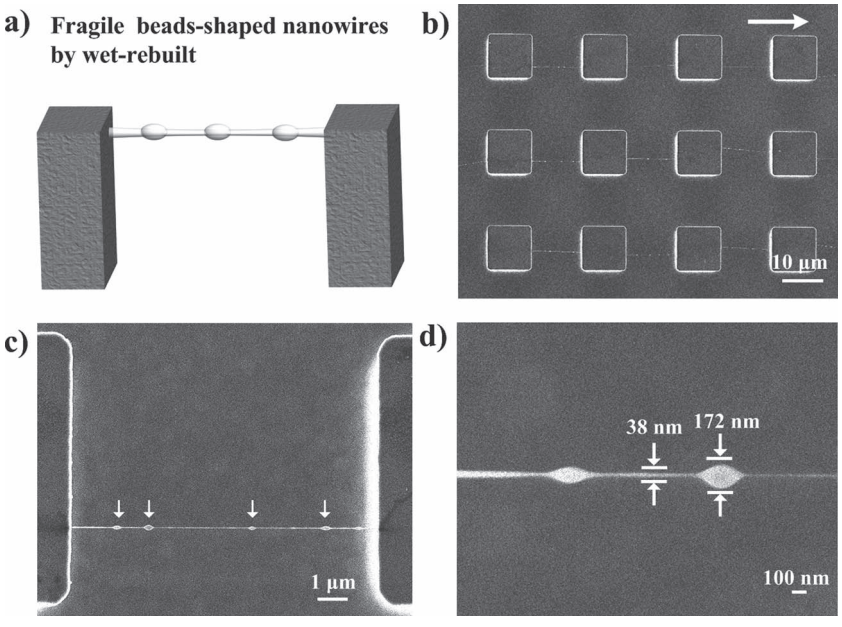

Figure 2. Strictly oriented bead-shaped nanowire arrays were prepared upon superhydrophobic pillar-structured silicon substrates at ultralow polymer concentration. a) Schematic illustration of Rayleigh-instability-driven bead-shaped nanowire arrays. b) Top view SEM image of as-prepared nanowire arrays arranged in one direction, exhibiting the guiding-effect of superhydrophobic pillar-structured surfaces. The white arrow shows the shrinkage directions of three-phase contact line (TCL) according to the droplet evaporation. c) Magnified image of (b), showing a single bead-shaped nanowire bridging neighbor micropillars. d) Magnified image of (c), exhibiting the sizes of beads and joint nanowire width. Ultrathin joint parts indicate low structural strength of Rayleigh-instability-driven bead-shaped nanowires.

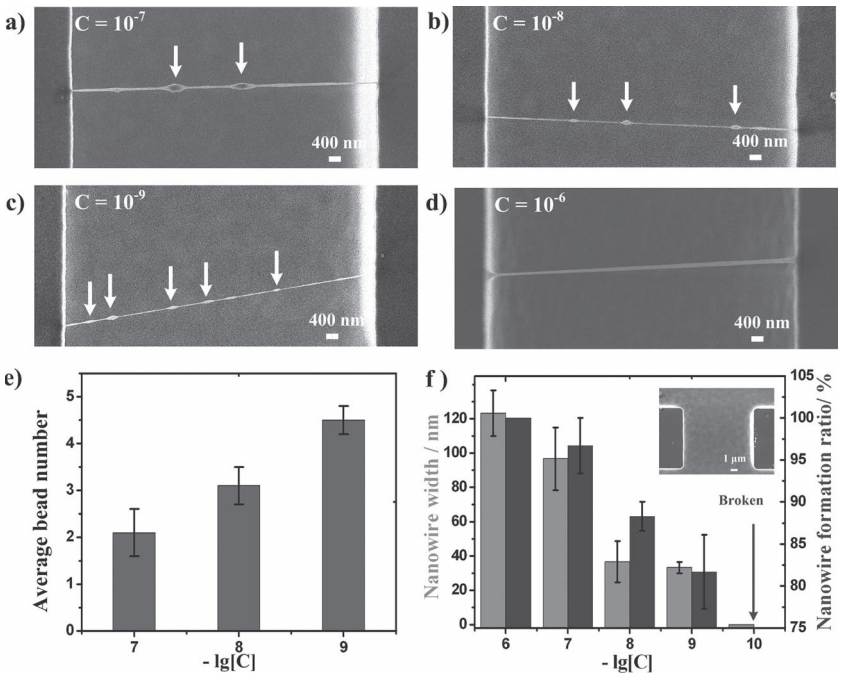

Figure 3. The dependence of average bead number, joint nanowire width, and nanowire formation ratio on the polymer concentration. Lower polymer concentration leads to more beads on the nanowires, but sacrifices their structural strength. Top view SEM images of bead-shaped nanowires generated at concentrations of a) 10^{-7}, b) 10^{-8}, c) 10^{-9} (w/w). d) As a control experiment, beads disappeared when the concentration was higher than 10^{-6}, indicating that the polymer concentration is the key to determine the occurrence/disappearance of beads on the nanowires. e) Statistical average bead number on the nanostructures prepared at diverse polymer concentration. f) The dependence of joint nanowire width and nanowire formation ratio on the polymer concentration. Lower concentration contributed to more beads on the nanowires but decreased structural strength, even no nanowires survived at 10^{-10} (w/w).

edges. Asymmetrically dispersed beads can be found along the thin nanowire. After carefully investigation of this nanostructure, the bead size was measured as ca. 172 nm while the width of joint nanowire was just ca. 38 nm (Figure 2d). These thin nanostructures were so fragile that they might break immediately once meeting a high-energy electronic beam in the SEM measurements.

The dependence of average bead number on polymer concentration has been studied, shown in **Figure 3**a–d. A series of PVF solutions at concentration from 10^{-6} to 10^{-10} (w/w) have been employed to generate bead-shaped nanowire arrays upon the same substrate. When the polymer concentration was lower than 10^{-7}, rare beads began to occur. Following the reduction of polymer concentration, average bead number increased from ca. 2 to ca. 4 on the nanowires (Figure 3e). Since the beads were contributed by the local aggregation of polymer chains under Rayleigh instability,[22] the possibility of such unusual aggregations would increase following the decrease of polymer concentration. In brief, more beads might occur along the nanowires at lower concentration. As a control experiment, beads disappeared when the concentration was higher than 10^{-6}, indicating polymer concentration was the key to decide the occurrence/disappearance of beads on the nanowires.

Notably, the nanowire width and nanowire formation ratio were investigated during the decrease of polymer concentration. Though reducing polymer quantity led to more beads on the nanowires, the width of joint nanowires became smaller (Figure 3f), indicating weaker structural cohesive force of these nanostructures. Therefore, as-prepared bead-shaped nanowires were fragile and easily broken, yielding decreasing nanowire formation ratio, even no nanowires survived at 10^{-10} concentration. It seems that bead-shaped nanowires driven by Rayleigh instability sacrifice structural strength, which greatly restricts their practical applications. Thus, exploring a novel way to prepare firm bead-shaped nanowires is still a challenge.

2.2. Firm Bead-Shaped Nanowire Arrays Utilizing PS Sphere as Bead Building Blocks

In our previous study, the concentration of PVF solution dominates the competition between capillary force (F_c) and structural cohesive force (F_s) inside liquid bridges, yielding high/low nanowire formation ratio.[19] Concentrated PVF solution might greatly increase F_s then break the nanowires while diluted polymeric solution leads to weak structural strength of 1D nanostructures. As a result, 10^{-3} (w/w) solution concentration is appropriate for generating firm nanowires with high formation ratio. Since Rayleigh instability can not happen at this high concentration, rigid PS spheres were mixed into PVF solution, allowing us to generate firm bead-shaped nanowire arrays on the same silicon substrate in one step.

Owing to the evaporation of water, PS spheres were fixed following the narrowing of liquid bridges. The diameter of PS spheres (ca. 320 nm) was larger than the nanowire width (ca. 130–150 nm), thus, such rigid spheres were suitable to serve as building blocks for the bead generation. **Figure 4**b shows the top view SEM image of PS-sphere-assisted bead-shaped nanowire arrays. As-prepared 1D nanostructures were oriented towards one direction over the whole image, exhibiting regularly aligning patterns that have not been reported by previous approaches.[5–16] From magnified image shown in Figure 4c, we can observe one bead-shaped nanowire bridging neighbor micropillars. After carefully investigation of this nanostructure, the bead size was ca. 376 nm while the width of joint nanowire was ca. 130 nm (Figure 4d). Since the width of PS-sphere-assisted bead-shaped nanowires (ca. 130 nm) is two times wider than that of Rayleigh-instability-driven nanowires (ca. 38 nm), the structural strength of nanostructures has been dramatically improved in this strategy, indicating firm bead-shaped nanowires that are suitable for the droplet collection.

Notably, the introduction of PS spheres into the PVF solution would improve the rheological behavior inside liquid bridges. The width of nanowires decreased following the reduced concentration of pure polymeric solution.[19] However, owing to the

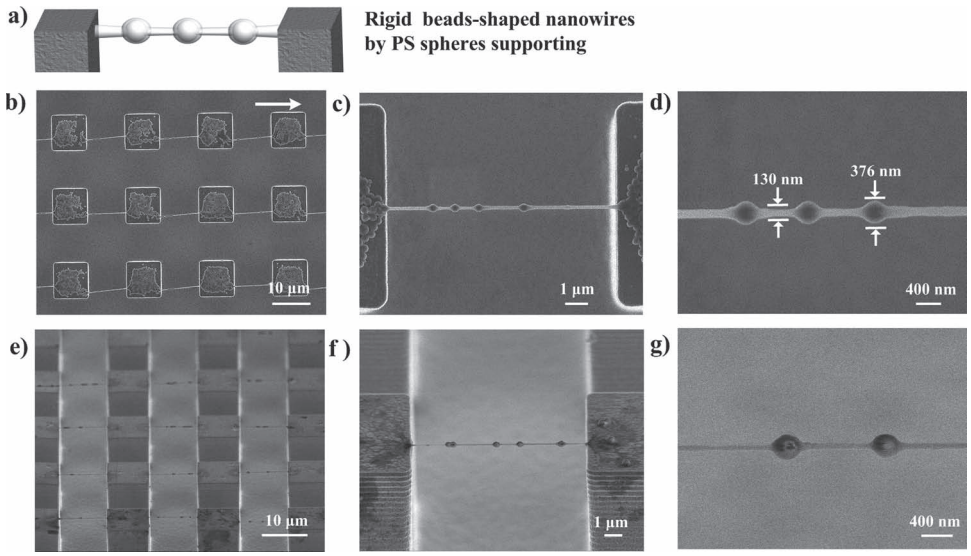

Figure 4. Suspended bead-shaped nanowires bridging neighbor micropillars with high structural strength by introducing PS spheres as the bead building blocks. The PVF concentration was fixed at 10^{-3}. a) Schematic illustration of PS-sphere-assisted bead-shaped nanowires. Rigid PS spheres were fixed inside the liquid bridges, yielding firm bead-shaped nanowires. b) Top view SEM image of horizontally oriented nanowire arrays. c) Magnified image of (b), showing a single bead-shaped nanowire bridging neighbor micropillars. d) Magnified image of (c), exhibiting larger sizes of beads and joint nanowire width. Because of the larger diameter of such nanostructures, the structural strength was improved accordingly. e) 45° incident angle view SEM images of bead-shaped nanowire arrays. The nanowires were far beyond the bottom surfaces, ca. 20 μm according to the micropillar height. f) Magnified image of (e), showing a single bead-shaped nanowire bridging neighbor micropillars' edges. g) Magnified image of (f), exhibiting the PS spheres was fixed by polymeric nanowires.

existence of rigid PS spheres, the width of joint parts along the bead-shaped nanowires won't follow the law. For example, the width of nanowires prepared at 10^{-6} (w/w) solution concentration is ca. 110–130 nm (Figure 3d) whereas the joint width of bead-shaped nanowires generated at 10^{-3} (w/w) is nearly the same (Figure 4d). These two results are incomparable because their rheological behaviors inside liquid bridges belong to different systems. Furthermore, since no surface charge or polar groups outside PS spheres, their interaction was quite weak. Following the narrowing of liquid bridges introduced by the evaporation of water, the PS spheres have been arranged randomly, yielding asymmetrically dispersed beads along the 1D nanostructures (Figure 4).

As shown in 45° incident angle SEM observation (Figure 4e), it was confirmed that the bead-shaped nanowires were suspended beyond the bottom surfaces (ca. 20 μm according to the micropillar height). Superhydrophobic micropillars played a key role in building such suspended bead-shaped nanostructures. When placing a PS-sphere-rich droplet upon the anti-wetting pillar-structured substrate, the droplet pinned on the surface but shrunk inwards. Owing to the adhesive property of micropillars, the unidirectional motion of droplet's TCL yielded regular liquid bridges parallel to the droplet moving direction. Because of the anti-wetting feature of micropillars, liquid bridges were suspended to connect neighbor micropillars rather than falling downwards. Then, the moving space of PS spheres inside liquid bridges was gradually limited following the water evaporation. Thus, PS spheres were fixed, yielding suspended bead-shaped nanowire arrays with high structural strength. Such asymmetrically dispersed beads could be found along the nanostructure in Figure 4f. From magnified image shown in Figure 4g, PS spheres were connected by joint nanowires and formed a strong bead-shaped nanowire bridging neighbor micropillars.

2.3. Tailoring the Bead Size

In order to control the bead size on the nanostructures, a series of PS spheres with different sizes at the same concentration were mixed with PVF solution (10^{-3}, w/w) to generate bead-shaped nanowire arrays. **Figure 5** reveals top view SEM images of as-prepared nanostructures utilizing PS spheres in diverse diameters. For small PS spheres (diameter of ca. 200 nm), far beyond our expectation, PS-sphere-aggregated 1D nanostructures are generated rather than bead-shaped nanowires (Figure 5a,b). When larger PS spheres (ca. 320 nm) were employed, regular bead-shaped nanowires could be formed. After careful observation, we found that plenty of PS spheres tend to aggregate upon neighbor micropillar tops (Figure 5d). Further increasing PS sphere diameter to ca. 430 nm, only a bead could be found along the nanowires. Most PS spheres aggregated on the micropillar tops rather than along the nanowires (Figure 5g,h). It seems that increasing PS sphere size led to their transport from the middle parts of the liquid bridges to the neighbor micropillar tops.

To explore the formation details of such bead-shaped nanowire arrays, in situ top-view optical observations have been performed, shown in **Figure 6**. With unidirectional motion of droplet's TCL, "U" shaped liquid films were generated between neighbor micropillars (Figure 6a,e,i), yielding PS-sphere-rich liquid bridges in horizontal direction. Owing to the evaporation of water, liquid bridges became narrower under the capillary

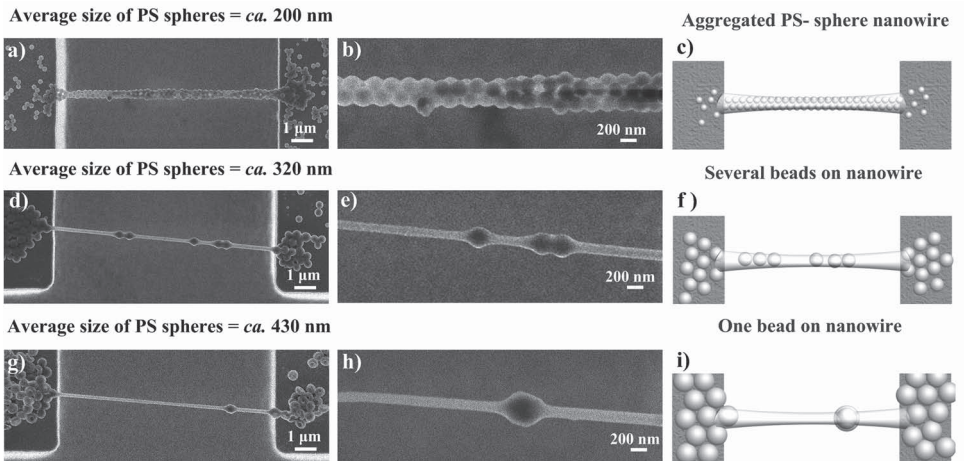

Figure 5. Tailoring the bead sizes by utilizing PS spheres with diverse diameters. Smaller PS spheres are easy to fix along the nanowires following the narrowing of liquid bridges, however, such aggregation of PS spheres yields the failure of bead-shaped nanowire formation. Larger PS spheres were repelled onto the micropillar tops during the liquid bridge evaporation, leaving rare big beads along the nanowires. Schematic illustration of the bead-shaped nanowire formation when utilizing PS spheres in c) ca. 200 nm, f) ca. 320 nm, and i) ca. 430 nm at the same concentration. The PVF concentration was fixed at 10^{-3}. Larger physical sizes of PS spheres indicate higher opportunity to be repelled from the middle part of liquid bridges to the micropillar tops. Top view SEM images of the nanostructures when utilizing PS spheres in a) ca. 200 nm, d) ca. 320 nm, and g) ca. 430 nm at the same concentration. Panels (b,e,f) are magnified images of (a,d,g), respectively. The bead sizes become larger following the increase of PS sphere sizes but the bead number decreased accordingly.

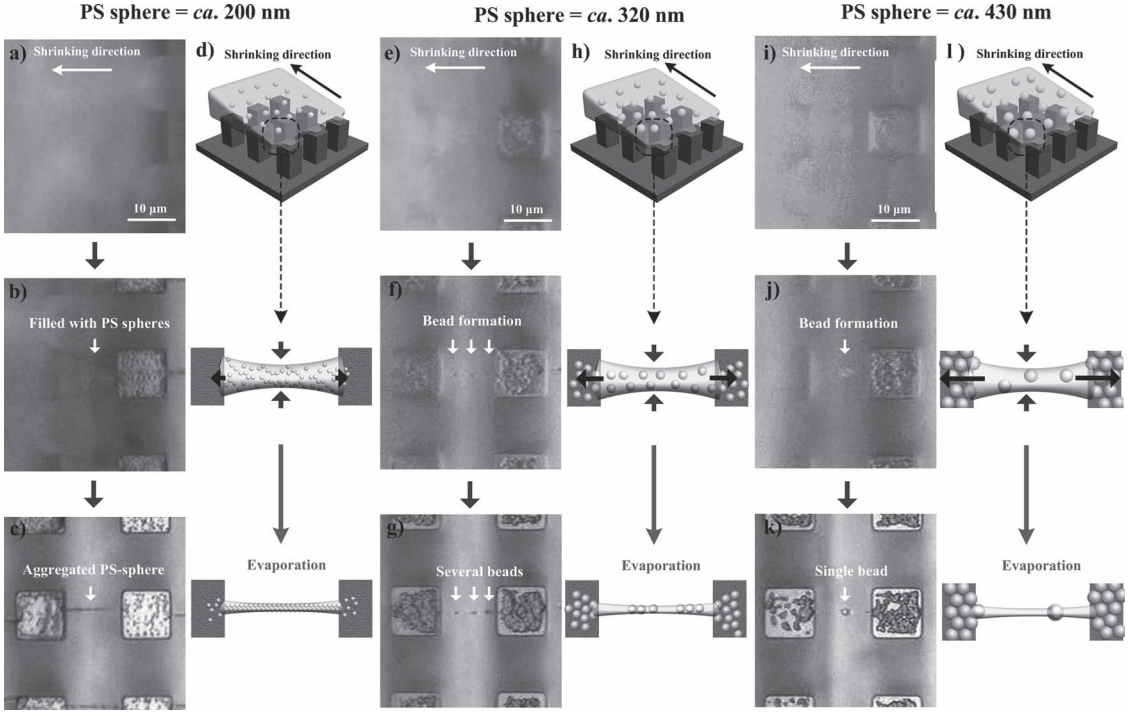

Figure 6. In situ top-view observations of bead-shaped nanowire forming processes with diverse bead sizes. Increasing PS sphere size led to their transport from the middle parts of the liquid bridges to the neighbor micropillar tops. a–c) The forming process of aggregated PS-sphere nanowires utilizing PS spheres (ca. 200 nm) doped PVF solution. Following the TCL shrinking, "U" shaped meniscus moved horizontally, yielding the generation of liquid bridges between adjacent micropillars. Small PS spheres were easy to fill inside the liquid bridges, which contributed to aggregated PS-sphere nanowires after the evaporation of water. e–g) When the physical size increased to ca. 320 nm, PS spheres were inclined to be repelled from the middle parts to the both sides of the liquid bridges. Thus, firm bead-shaped nanowires could be formed accordingly. i–k) When using larger PS spheres (ca. 430 nm) to generate bead-shaped nanowires, few beads have been found along the 1D nanostructures whereas most PS spheres stayed upon the micropillar tops. Panels (d,h,l) are the schematic illustrations of (a–c), (e–g), (i–k), respectively.

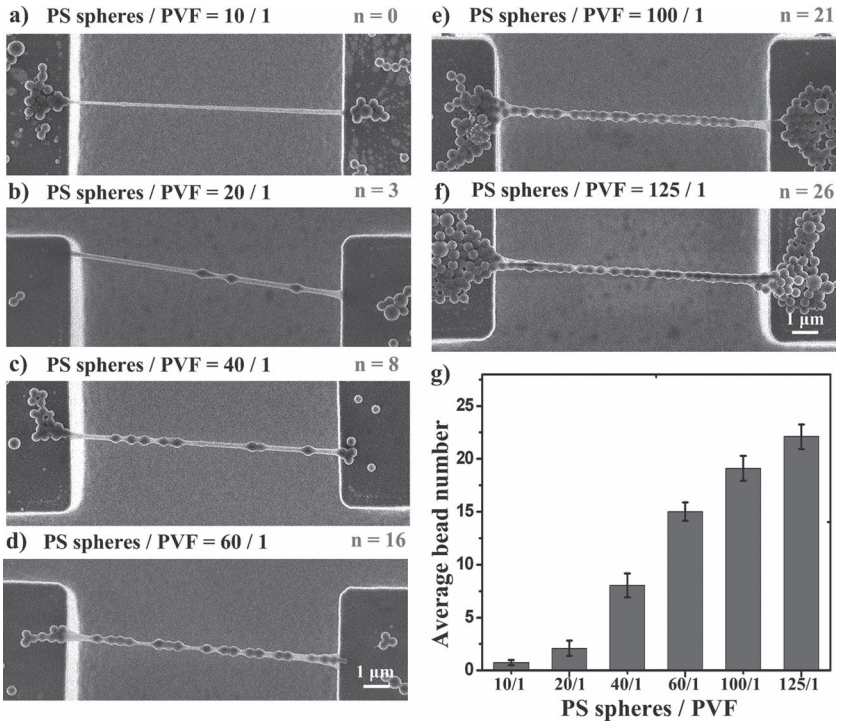

Figure 7. The dependence of average bead number on the PS-spheres/PVF ratio. The PVF concentration was fixed at 10^{-3}. Larger PS sphere concentration leads to more beads along the nanowires. a–f) Top view SEM images of bead-shaped nanowires bridging neighbor micropillars employing diverse PS-spheres/PVF ratio. When the ratio was below 10 (w/w), PS spheres were inclined to staying on the micropillar tops rather than the nanowires, yielding smooth nanowires. As the ratio increasing from b) 20 to e) 100, the bead number on nanowires was dramatically enhanced. f) At the ratio of 125, the beads were in contact with each other along the entire nanowires. g) Statistical average bead number on the nanostructures prepared at diverse PS-spheres/PVF ratio.

force, especially in the middle part (see Figure 6b,f,j). Since small PS spheres owned the similar physical size (ca. 200 nm) to that of nanowire width (ca. 130–150 nm), they would be fixed and aggregated along the nanostructures even the narrowing of liquid bridges. Thus, PS-sphere-aggregated 1D nanostructures were generated rather than bead-shaped nanowires (Figure 6c). However, larger physical size of PS spheres were easy to suffer the pressure caused by the narrowing of liquid bridges, indicating higher opportunity to be repelled from the middle part of liquid bridges to adjacent micropillar tops. Thus, PS spheres of ca. 320 nm contributed to a few beads along the 1D nanostructures whereas most of them were repelled and stayed on the neighbor micropillar tops (Figure 6g). Following the increase of rigid PS sphere diameter to ca. 430 nm, the capillary force introduced pressure owned more time to repel them to the micropillar tops before the solidification of liquid bridges, leaving rare bead along the nanowires (Figure 6k). In brief, larger PS spheres would prefer to position on micropillar tops instead of nanowires due to the repel tendency caused by the pressure in the liquid bridge narrowing process. Thus, it is still a tough problem to tailor the bead size of bead-shaped nanowires by utilizing PS spheres with diverse diameters. Approaches to generate aligning bead-shaped nanowires with tunable bead size are under future studying.

2.4. Tailoring the Bead Number

The dependence of average bead number on the PS-sphere/PVF ratio was investigated. Higher ratio led to more beads fixed on the nanowires. **Figure 7**a–f shows the top view SEM images of bead-shaped nanowires prepared at diverse PS-sphere/PVF ratios. The PVF concentration was fixed at 10^{-3} (w/w). When the ratio was below 10 (w/w), PS spheres were inclined to staying on the micropillar top rather than the nanowires, yielding smooth nanowires. As the ratio increasing from 20 to 100, the bead number on nanowires was dramatically enhanced. Especially at the ratio of 125, the beads contacted to each other along the whole nanowires. Since the beads were constructed by PS spheres, higher PS spheres quantity indicate larger possibility for fixing such nanounits inside liquid bridges, yielding more beads upon the nanowires after the water evaporation (Figure 7g). It is feasible to control the bead number by tailoring the PS-sphere/PVF ratio.

2.5. Directional Droplet Collection Upon the Bead Nanostructures

In our previous studies, bead-shaped structures owned the unique ability to directional drive tiny drops and collect coalesced microdroplets when placed in mist.[15] Surface energy gradients and differences in Laplace pressure mainly take charge in driving tiny drops from joint parts towards the beads.[23] Then, diverse drops coalesced on the beads, yielding larger droplets for water collection. As shown in **Figure 8**, the process of fog collection on a bead-shaped nanowire was observed from an optical microscopy. A nanowire with joint width of ca. 140 nm and bead size of ca. 380 nm was bridging neighbor micropillars (Figure 8a). After the fog blowing, tiny water drops condensed randomly on the nanowire and began to move towards the bead under the Laplace pressure differences (Figure 8b).[23] The droplet size on the bead increased from less than 0.4 μm to ca. 3 μm within 12 s while the nanowire width remained the same, indicating the directional droplet collection by the bead structure (Figure 8c). Regular alignment of bead-shaped nanowires played a key role in protecting the drops' coalescence on the beads. Cross-link/overlapping bead-shaped nanowires in random alignment might bring too close physical contact between the beads, indicating a misguiding of drops to coalesce upon the beads. In brief, aligning bead-shaped nanowires were able to directionally collect microdroplets in mist while the alignment of bead-shaped nanowires protected this process.

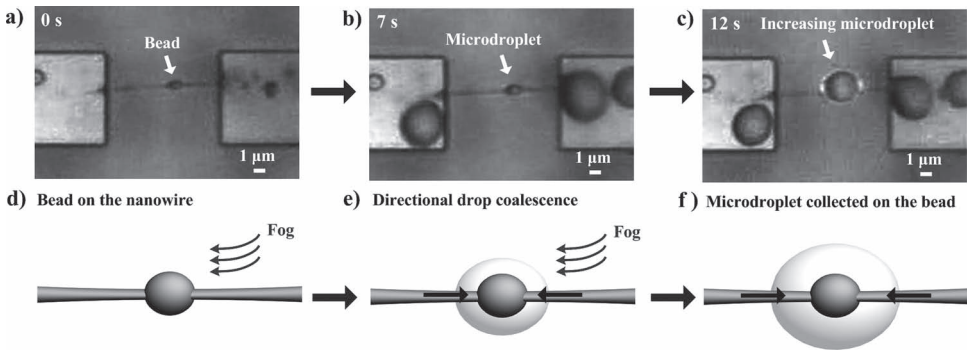

Figure 8. The detailed collection process of microdroplets upon the bead structured nanowire. a–c) In situ optical microscopy images of the directional water collection process on the bead. a) A nanowire with joint width of ca. 140 nm and bead size of ca. 380 nm was bridging neighbor micropillars. b) Following the fog blowing, tiny water drops condensed randomly on the nanowire and began to move towards the bead under the Laplace pressure differences. c) The droplet size on the bead increased from less than 0.4 μm to ca. 3 μm within 12 s, while the nanowire width remained the same, indicating the directional droplet collection by the bead structure. Panels (d–f) are schematic illustrations of (a–c), respectively.

3. Conclusions

In summary, we have successfully fabricated elaborately programmed bead-shaped nanowire arrays upon highly adhesive superhydrophobic pillar-structured silicon substrates. Our results show that Rayleigh instability could introduce bead-shaped nanowires at the cost of structural strength. Thus, firm bead-shaped nanowire arrays were generated by utilizing PS spheres serving as bead building blocks. The bead number was tunable by tailoring the PS-sphere/PVF ratio. Furthermore, bead-shaped nanowires own the unique ability to directional drive tiny drops and collect coalesced microdroplets when placed in mist. Following the increase of environmental humidity, the bead-shaped nanowires showed a segmented swelling behavior in the "bead" parts whereas the "joint nanowire" parts remained the same. Such elaborately aligning bead-shaped nanowire arrays are of great significance in highly integrated functional devices and are anticipated to bring about many important properties and applications.[24,25]

4. Experimental Section

Ordered Pillar-Structured Substrate Fabrication: Silicon wafers (10 cm. diameter, N type doped with phosphorus, <100> oriented, 525 μm thick) were structured by standard photolithography techniques. Pillar-structured silicon substrates with tunable pillar top areas, pillar gaps and pillar top shapes could be fabricated. After resist stripping (Microposit Remover 1165), the substrates were cleaned by ethanol and acetone, waiting for the chemical modification process.

Surface Modification: The high-adhesively superhydrophobic pillar-structured silicon substrates were generated by silanizing the silicon substrates with heptadecafluorodecyltrimethoxysilane (FAS) in a decompression environment at room temperature for 24 h and then heated at 80 °C for 3 h, yielding in reproducible homogeneous highly hydrophobic surfaces.

Preparation of Aligning Bead-Shaped Nanowire Arrays: For Rayleigh-instability-driven bead-shaped nanowires, droplets (4 μL) of diluted PVF aqueous solutions at diverse concentrations (10^{-6} to 10^{-10}, w/w) were carefully placed onto superhydrophobic pillar-structured silicon substrates. Owing to the high adhesion of such a surface, regular liquid bridges could be generated between neighbor micropillars. Owing to Rayleigh instability effect, aligning bead-shaped nanowire arrays were thus generated at the cost of structural strength. For PS sphere assisted bead-shaped nanowires, PS spheres with diverse sizes were mixed with PVF at different ratio. Then, the nanowire formation process could be performed under the similar conditions.

Directional Droplet Collection Upon the Bead-Shaped Nanowires: Bead-shaped nanowire arrays were fixed under the object lens of an optical microscopy. Numerous tiny water drops generated by an YC-E350 ultrasonic humidifier (Beijing YADU Science and Technology Co., Ltd.) were introduced into the sample and condensed on the bead-shaped nanowires. The whole process was recorded by the optical microscopy and CCD components. In every figure showing directional motion of tiny water drops, time zero was chosen to be the frame in which condensed drops began to visually appear.

Instruments and Characterization: The structures of suspended bead-shaped nanowire arrays were investigated by scanning electron microscopy (SEM, JEOL, JSM-6700F, Japan) at accelerating voltage of 3.0 kV. Static contact angles were measured on a dataphysics OCA20 contact-angle system at ambient temperature. The average CA was obtained by measuring more than five different positions of the same sample. The process of droplet collection and evaporation upon the beads was investigated through an optical microscope (Vision Engineering Co., UK), which was coupled to a CCD camera and connected to a desktop computer.

Acknowledgements

The authors acknowledge the financial support from the National Research Fund for Fundamental Key Projects (2009CB930404, 2010CB934700, 2011CB935700, 2012CB933200), National Natural Science Foundation (20974113, 21071148, 20920102036, 21121001, 91127025, 51173099), and the Key Research Program of the Chinese Academy of Sciences (KJZD-EW-M01).

Received: April 5, 2012
Revised: June 6, 2012
Published online: June 25, 2012

[1] H. Yan, H. S. Choe, S. W. Nam, Y. J. Hu, S. Das, J. F. Klemic, J. C. Ellenbogen, C. M. Lieber, *Nature* **2011**, *470*, 240.
[2] H. Bai, J. Ju, R. Z. Sun, Y. Chen, Y. M. Zheng, L. Jiang, *Adv. Mater.* **2011**, *23*, 3708.
[3] H. Bai, X. L. Tian, Y. M. Zheng, J. Ju, Y. Zhao, L. Jiang, *Adv. Mater.* **2010**, *22*, 5521.
[4] X. L. Tian, Y. Chen, Y. M. Zheng, H. Bai, L. Jiang, *Adv. Mater.* **2011**, *23*, 5486.

[5] S. J. Hurst, E. K. Payne, L. D. Qin, C. A. Mirkin, *Angew. Chem. Int. Ed.* **2006**, *45*, 2672.
[6] C. J. Su, C. Y. Chen, H. L. Chen, V. A. Ivanov, *J. Phys.: Conf. Ser.* **2011**, *272,* 012002.
[7] L. A. Morozova-Roche, V. Zamotin, M. Malisauskas, A. Ohman, R. Chertkova, M. A. Lavrikova, I. A. Kostanyan, D. A. Dolgikh, M. P. Kirpichnikov, *Biochemistry* **2004**, *43*, 9610.
[8] J. H. Zhan, Y. Bando, J. Q. Hu, Z. W. Liu, L. W. Yin, D. Golberg, *Angew. Chem. Int. Ed.* **2005**, *44*, 2140.
[9] E. Kang, G. S. Jeong, Y. Y. Choi, K. H. Lee, A. Khademhosseini, S. H. Lee, *Nat. Mater.* **2011**, *10*, 877.
[10] J. E. Oliveira, E. A. Moraes, R. G. F. Costa, A. S. Afonso, L. H. C. Mattoso, W. J. Orts, E. S. Medeiros, *J. Appl. Polym. Sci.* **2011**, *122*, 3396.
[11] J. H. Park, P. V. Braun, *Adv Mater.* **2010**, *22*, 496.
[12] X. L. Tian, H. Bai, Y. M. Zheng, L. Jiang, *Adv. Funct. Mater.* **2011**, *21*, 1398.
[13] J. F. Zheng, A. H. He, J. X. Li, J. A. Xu, C. C. Han, *Polymer* **2006**, *47*, 7095.
[14] Y. I. Yoon, H. S. Moon, W. S. Lyoo, T. S. Lee, W. H. Park, *J. Colloid Interface Sci.* **2008**, *320*, 91.
[15] Y. M. Zheng, H. Bai, Z. B. Huang, X. L. Tian, F. Q. Nie, Y. Zhao, J. Zhai, L. Jiang, *Nature* **2010**, *463*, 640.
[16] H. Bai, R. Z. Sun, J. Ju, X. Yao, Y. M. Zheng, L. Jiang, *Small* **2011**, *7*, 3428.
[17] Y. Huang, X. F. Duan, Q. Q. Wei, C. M. Lieber, *Science* **2001**, *291*, 630.
[18] X. F. Duan, C. M. Niu, V. Sahi, J. Chen, J. W. Parce, S. Empedocles, J. L. Goldman, *Nature* **2003**, *425*, 274.
[19] B. Su, S. T. Wang, J. Ma, Y. C. Wu, X. Chen, Y. L. Song, L. Jiang, *Adv. Mater.* **2012**, *24*, 559.
[20] B. Su, S. T. Wang, Y. C. Wu, X. Chen, Y. L. Song, L. Jiang, *Adv. Mater.* **2012**, *24*, 2780.
[21] S. T. Wang, L. Jiang, *Adv. Mater.* **2007**, *19*, 3423.
[22] P. P. Bhat, S. Appathurai, M. T. Harris, M. Pasquali, G. H. McKinley, O. A. Basaran, *Nat. Phys.* **2010**, *6*, 625.
[23] E. Lorenceau, D. Quere, *J. Fluid Mech.* **2004**, *510*, 29.
[24] L. Fu, Z. M. Liu, Y. Q. Liu, B. X. Han, P. G. Hu, L. C. Cao, D. B. Zhu, *Adv. Mater.* **2005**, *17*, 217.
[25] G. Z. Shen, P. C. Chen, Y. Bando, D. Golberg, C. W. Zhu, *Chem. Mater.* **2008**, *20*, 6779.